Multiobjective Hypersonic Entry Aeroshell Shape Optimization

John E. Theisinger* and Dr. Robert D. Braun†
Georgia Institute of Technology, Atlanta, Georgia, 30332-0150

A capability has been developed that utilizes multiobjective optimization to identify hypersonic entry aeroshell shapes that will increase landed mass capability. Aeroshell shapes are parameterized using non-uniform rational B-splines to generate complete aeroshell surfaces. Hypersonic aerodynamic objectives and constraints are computed by numerically integrating pressure coefficient distributions obtained using Newtonian flow theory. An integrated optimization environment is created using iSIGHT with single- and multiobjective evolutionary algorithms. Results are presented based on optimization using constraints derived from the aeroshell for the Mars Science Laboratory mission. Resulting solutions clearly demonstrate the trade-offs between drag-area, static stability, and volumetric efficiency for this particular mission.

Nomenclature

A	=	reference area
C_DA	=	drag-area (= D/ q_∞)
C_LA	=	lift-area (= L/ q_∞)
C_M	=	pitching moment coefficient
C_MAl	=	pitching moment per unit freestream dynamic pressure (= M/ q_∞)
C_p	=	pressure coefficient
D	=	drag force or diameter
L/D	=	lift-to-drag ratio
L	=	lift force or length
l	=	reference length
M	=	pitching moment
m	=	mass
$\mathbf{n}$	=	surface normal unit vector
q_∞	=	freestream dynamic pressure
r_n	=	nose radius
$\mathbf{V}_\infty$	=	freestream velocity vector
α	=	angle of attack
β	=	ballistic coefficient
θ	=	half-cone angle

I. Introduction

AEROSHELLS are designed to deliver payloads safely through a planetary atmosphere, protecting the payload from the high aerodynamic heating and loads encountered during hypersonic entry, descent, and landing (EDL). The aeroshell also provides the aerodynamic drag force necessary for deceleration, dissipating approximately 90% of the EDL system's kinetic energy from the point of atmospheric interface. The aeroshell is designed to provide these functions with minimum possible mass so that useful landed mass can be maximized.

An aeroshell generally consists of a forebody (or heatshield), which faces the flow, and a backshell, which completes the encapsulation of the payload. The specific shape of a particular aeroshell is driven by EDL performance requirements and thermal/structural limitations. Four different aeroshell shapes are shown in Fig. 1: the Viking-era 70° sphere-cone, the Mars Microprobe, the Aeroassist Flight Experiment (AFE), and a swept biconic

* Graduate Research Assistant, Daniel Guggenheim School of Aerospace Engineering, AIAA Student Member
† David and Andrew Lewis Associate Professor of Space Technology, Guggenheim School of Aerospace Engineering, AIAA Associate Fellow.

design. Primary drivers of these aeroshell designs include drag, stability, nonequilibrium aerothermodynamics, and radiative heating, respectively. This diversity in configurations is a direct result of differing mission and flight systems requirements – that is, form has followed function in every case.

Figure 1. Various aeroshell shapes. [1-4]

Fundamentally, the drag-area (C_DA) represents the amount of drag force that an aeroshell is capable of generating at a given free-stream condition (i.e., D/q_∞). During the hypersonic EDL phase, this drag force provides the means of deceleration, suggesting that C_DA should be maximized for a given system mass (m). The ballistic coefficient is an aeroshell performance parameter that embodies this principle, relating inertial and drag forces as shown in Eq. (1).

$$\beta = \frac{m}{C_D A} \tag{1}$$

A higher β (higher mass per unit drag-area) causes EDL events to occur at lower, denser portions of the atmosphere, reducing landed elevation capability and timeline margin. Additionally, peak heat rate and integrated heat load are higher, causing an increase in the thermal loads that the entry system must be designed to accommodate. Accommodating these loads generally leads to a heavier thermal protection system (TPS) and support structure, reducing the useful landed mass capability of the EDL system. While a high C_DA can be achieved by making the aeroshell forebody as blunt as possible, static stability must also exist in order to maintain this high-drag attitude. Static stability requires a certain amount of sweep in the aeroshell forebody, in effect making the shape less blunt. This trade-off between drag and stability is fundamental in aeroshell shape design.

Another important aeroshell performance parameter is the lift-to-drag ratio (L/D). A body of revolution, symmetric about its forward axis, will have an L/D equal to zero while flying at a 0° angle of attack (AOA or α). A body of revolution flying at a non-zero AOA, or an asymmetric body, however, can produce a non-zero L/D. Trim stability can be achieved at this AOA by either offsetting the center of gravity (CG) of the aeroshell or by using an aerodynamic body flap to counteract restoring moments. Once again, it is critical that the aeroshell be statically stable at this trim attitude. Motivations for achieving a non-zero L/D aeroshell shape and/or attitude include:

- To relax the allowable approach navigation requirements (i.e., enabling a larger entry corridor).
- To reduce the deceleration loads.
- To mitigate atmospheric density and wind uncertainties.
- To improve landing accuracy.
- To increase parachute deployment altitude, enabling a higher surface elevation landing site or adding timeline margin.
- To execute a plane change or to provide a crossrange capability.

While a non-zero L/D has distinct advantages, care must be taken not to shape the aeroshell such that L/D is created at the expense of reducing C_DA and therefore increasing β. This risk can be seen more clearly in Eq. (2) where L/D is written in terms of C_DA.

$$L/D = \frac{C_L A}{C_D A} \tag{2}$$

Fundamentally, the L/D required of the aeroshell should be set no higher than that required to satisfy the mission requirements. An ideal aeroshell shape would achieve this specified L/D while maximizing C_DA (thereby minimizing β) and be statically stable at the trim attitude. This enables the aeroshell to perform as needed while sacrificing as little critical drag-area as possible – preserving its capability to deliver a payload to the planetary surface safely and effectively. Such a problem is naturally solved through aeroshell shape optimization.

In addition to these aerodynamic considerations, the aeroshell should have minimum mass so that payload mass can be maximized. The aeroshell structure and TPS weight thus directly impact the capability to deliver certain

landed payload masses. As mentioned previously, minimizing β will reduce heating; however, this is a trajectory effect and the local aerothermodynamic environment will be defined at every point on the surface by the aeroshell geometry (e.g., local curvature). Other geometric considerations include the volumetric efficiency (affecting payload packaging) and the overall aeroshell size, which must satisfy launch vehicle shroud size restrictions. Ultimately, there are many objectives to be optimized and constraints to be met when considering the shape of an aeroshell.

These objectives cannot be simultaneously optimized to their fullest extent – some level of trade-off will be required. The conflicting nature of these objectives suggests that multiobjective optimization methods be employed that allow the consideration of several objectives simultaneously while satisfying all necessary constraints. Therefore, given a set of mission requirements that define constraints (such as *L/D*, volume, and size), the aeroshell shape can be optimized in a multiobjective sense.

II. Methodology

This work is separated into three main components: hypersonic aerodynamic analysis, shape parameterization, and multiobjective optimization. The following sections detail each component and discuss how these components were integrated to create the capability to perform multiobjective aeroshell shape optimization at the conceptual design level.

A. Hypersonic Aerodynamics

Routines were coded in MATLAB to determine the aerodynamic quantities for a given shape using basic Newtonian impact theory. Sideslip is not modeled; aeroshells are only allowed to vary in AOA. Aeroshells are required to be symmetric across the pitch plane, forcing the rolling and yawing moments to be zero for all angles of attack. In locating the center of gravity (CG) of the aeroshell, a uniform packaging density is assumed, which effectively places the axial CG location at the volume centroid of the aeroshell. The lateral CG offset required to trim an aeroshell is determined based on the computed forces and moments about this centroid. Static longitudinal stability is assessed using a finite difference calculation of the pitching moment about the offset CG to calculate this derivative. Lateral and directional stability are not considered in this work, nor is dynamic stability. Note that a constant $C_{p,max}$ value of two was used in all aerodynamic analyses, consistent with the assumptions of basic Newtonian impact theory. Employing modified Newtonian aerodynamics will not affect the aerodynamic trends associated with aeroshell shape changes unless trajectory coupling is included in the optimization. However, even in these cases, the hypersonic aerodynamic characteristics of the aeroshell will only be a weak function of trajectory due to the Mach number independence principle. Therefore, this work is a fitting application for straight Newtonian flow theory.

B. Shape Parameterization

The proper choice of shape parameterization is that which yields an appropriate mix of design freedom and computational efficiency. In terms of optimization, it is most computationally efficient to keep the number of design variables to a minimum; however, more design freedom typically requires a larger number of design variables. Because aeroshell shapes can vary in complexity based on design requirements, the goal here is to select an aeroshell shape parameterization that will allow for sufficient design freedom with a minimum number of design variables. The following shape parameterizations were explored: analytic shapes, spline surfaces of revolution, and general spline surfaces.

1. *Analytic Shapes*

Analytic shapes provide the ability to define an aeroshell shape in terms of a few geometric parameters, minimizing the number of design variables for optimization while allowing for smooth, manufacturable, and realistic shapes to be designed and analyzed. The main drawback to this approach is its lack of design freedom: aeroshell shapes are inherently restricted to a specific family, greatly limiting the variety and generality of possible designs. A priori, there is no reason to expect an optimal aeroshell shape to take a strictly analytic form for the general design problem.

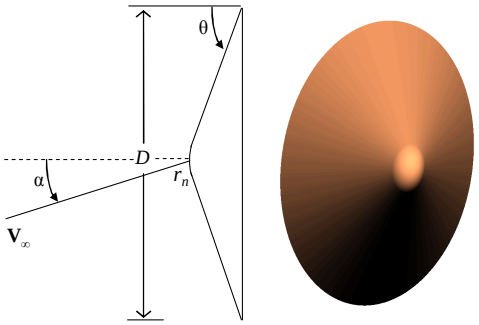

Figure 2. Sphere-cone forebody shape.

For example, the sphere-cone forebody is parameterized in terms of four design variables: the nose radius (r_n), cone angle (θ), maximum diameter (*D*), and the AOA (α), as shown in Fig. 2. A representative sphere-cone forebody is also shown in this figure. Typically, the backshell that completes this aeroshell is conical or a combination of several conical

frustums; however, some designs have even employed hemispherical shells (see Fig. 1). Additionally, a finite shoulder radius must be included as a shape parameter to join the forebody and backshell and complete the overall aeroshell. In total, such an aeroshell parameterization would involve roughly half a dozen design variables.

2. Spline Surfaces of Revolution

To expand the range of possible shapes, forms with increasing levels of geometric control are implemented. The first improvement is to examine aeroshells represented as surfaces of revolution (SORs). An axial profile is first created from a series of control points confined within certain axial bounds. This limited range of motion prevents control points from crossing and producing twisted shapes. Additionally, generating a closed body with a specified length requires a completely fixed point at the nose of the profile and an axially-fixed point at the end of the profile, respectively. Such an arrangement is shown in Fig. 3.

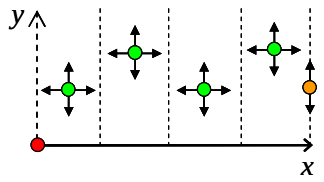

Figure 3. SOR profile control points.

Once control points are positioned, a specific curve representation describes the SOR profile. The axial profile is then rotated by 360° about the centerline to form an axisymmetric surface. The most basic method for generating axial profiles is a direct-mesh approach in which the profile is represented by a linear interpolation of the control points. The direct-mesh SOR is an intuitive choice because the profile simply connects the control points. However, this approach results in faceted shapes, which may be undesirable for general shape design and optimization. In order to approximate a smooth profile, a large number of control points would be required, a circumstance which becomes computationally burdensome for optimization routines. In order to allow for smooth axial profiles without adding a large number of control points, a functional curve form is used. A parametric curve is ideal because parametric forms have the ability to represent bounded and closed curves.

B-spline curves are parametric curves that are defined by weighting a given set of control points with parametric basis functions. As such, B-spline curves are defined through the placement of control points and the definition of a knot vector, which dictates the parameter ranges over which each control point has an influence. An advantage of using the B-spline formulation is the convex hull property, which ensures that the curve will lie entirely within the polygon created by the control points. Additionally, the variation-diminishing property dictates the maximum amount of curve oscillation within the convex hull. Given these two properties, the designer can readily predict the shape of a curve based on its control polygon.

While SORs can be used to represent analytic shapes that are axisymmetric, such as the sphere-cone forebody, they also allow a broad range of other, non-analytic shapes. The control points, along with the AOA, are the design variables used for shape optimization. Despite the significant improvement in design freedom over analytic shapes, all SOR aeroshell shapes will be axisymmetric. Again, there is no reason to expect an optimal aeroshell shape to be strictly axisymmetric for the general design problem.

3. General Spline Surfaces

Rather than simply look to families of non-axisymmetric cross sections, a surface representation was sought that has the capability to treat the aeroshell as a closed, free-form surface for shape design. To this end, non-uniform rational B-spline (NURBS) surfaces were implemented.

A bi-parametric, cubic by quadratic NURBS surface formulation was found to give the desired amount of design flexibility for roughly 20 design variables, including AOA. Shifting from a spline SOR to a spline surface formulation introduces several additional considerations. First, the control points defining the surface must each now be confined to a three-dimensional range of coordinates in order to prevent twisted shapes from being generated. This is a natural extension of the axial bounds placed on the control points used to generate axial profiles for the SORs. Only half of the aeroshell surface needs to be defined since bi-lateral symmetry (across the pitch plane) is strictly enforced. Control points are distributed axially from the apex of the aeroshell forebody to the apex of the aeroshell backshell, generating five convex axial control point profiles that define one half of the aerohsell. The forebody and backshell apex can be moved anywhere vertically along the forebody and backshell of the aeroshell, respectively. A NURBS surface is therefore defined by multiple axial profiles rather than a single profile as in the SOR case. The fact that NURBS can represent conic sections and quadric surfaces exactly provides one particular advantage in terms of constraint enforcement. Each cross-section is constrained within a circular envelope, which limits the maximum radius of the aeroshell along its entire length. Thus, the constraint on aeroshell

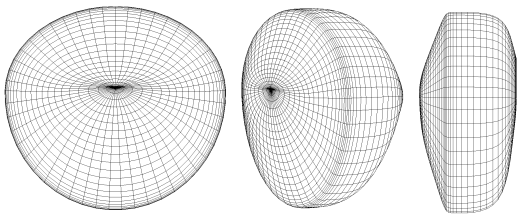

Figure 4. NURBS surface front, oblique, and side views.

packaging within the launch vehicle shroud can easily be accommodated via the NURBS representation. Once a maximum length and a maximum radius are defined, control point placement yields a complete aeroshell surface. An arbitrary NURBS surface generated based on this framework is shown in Fig. 4.

C. Multiobjective Aeroshell Shape Optimization

As discussed previously, the overarching objective is to maximize the aeroshell C_DA while achieving a specified L/D. However, if C_DA were to be maximized unchecked, the result would be the trivial solution of a flat plate at an angle of attack. The impact of maximizing C_DA on other aeroshell characteristics, some brought in by other disciplines, must be considered concurrently. Such a need requires multiobjective optimization. In addition to drag-area, the static longitudinal stability, packaging, and overall system mass of the aeroshell are all potential objectives for aeroshell shape optimization.

1. Aerodynamic Objectives and Constraints

As previously outlined, Newtonian impact theory is used to determine the C_p distribution over the entire aeroshell surface for a given AOA. After numerical integration, the C_DA and C_LA are obtained for the aeroshell and L/D is computed using Eq. (2). Similarly, C_MAl is obtained directly through numerical integration over the aeroshell surface mesh, referenced to the centroid of the aeroshell. From this value of C_MAl, the lateral CG offset that is required to trim the aeroshell at this AOA is computed. Based on this offset CG, a central finite difference calculation is made in order to determine the derivative of C_MAl with respect to AOA: $(C_MAl)_\alpha$. Using the convention of positive pitching moment being nose-up, a negative value of $(C_MAl)_\alpha$ is required for static longitudinal stability. Any of these quantities can then be used as aerodynamic objectives or constraints in performing aeroshell shape optimization. The current motivation prescribes an optimization problem in which L/D is used as a constraint, C_DA is maximized, required lateral CG offset is minimized (in absolute value), and static stability is maximized by minimizing the quantity $(C_MAl)_\alpha$.

2. Geometric Objectives and Constraints

Other objectives and constraints, such as volume, volumetric efficiency and aeroshell mass due to structure and TPS require analysis of the aeroshell geometry. Once the aeroshell geometry has been defined and represented numerically, volume and surface area can easily be computed. A constraint on volume can then be checked directly, while additional objectives can be derived from other combinations of aeroshell volume and surface area. The goal in formulating objectives for structural mass and TPS mass is to match the trends associated with changes in aeroshell shape.

The structural mass of an aeroshell will be directly proportional to the size of the aeroshell – particularly the surface area. Also, since an aeroshell is essentially a pressure vessel, the more its shape deviates from spherical, the more internal support structure will be required for rigidity. For a similar reason, aerodynamic moments imposed on lifting aeroshells will require additional internal structural supports. Therefore, structural mass will be inversely proportional to the volumetric efficiency, defined in Eq. (3), where V is the aeroshell volume and S is the aeroshell surface area.[8]

$$\eta_V = \frac{6\sqrt{\pi}V}{S^{3/2}} \tag{3}$$

Note that η_V is maximized at unity for a sphere, which is the aeroshell shape with the best volumetric efficiency. As such, slender aeroshell shapes will have a lower η_V and therefore a larger structural mass than blunt aeroshells. Additionally, lower η_V indicates a poorer ability to package payload into the aeroshell.

In the current work, an objective related to TPS mass is not included, although it is assumed that maximizing C_DA (thereby reducing β) will reduce heating. The TPS mass of an aeroshell is directly proportional to (1) the heat rates and heat load encountered during entry, and (2) the wetted surface area of the aeroshell. The total heat rate consists of a convective and a radiative heat rate component. At the stagnation point, these heat rates are proportional to the effective nose radius of the aeroshell and the shock stand-off distance at the stagnation point, respectively. Note that a larger effective nose radius reduces the convective heating component, but increases the shock stand-off distance, therefore increasing the radiative heating component. In terms of minimizing the total heat rate, these two components generally conflict; however, in most robotic missions the convective heat rate dominates, allowing focus to be placed on maximizing the effective nose radius of the aeroshell. For very high-speed Earth entries, such as return from the moon, radiative heating has a more significant impact and must be considered in the design of the aeroshell shape. Both the wetted surface area and the effective nose radius will depend on the specific shape of the aeroshell and its attitude during trimmed flight. Note that using Newtonian impact theory, none of the aeroshell surface area that lies in the shadow region is considered wetted by the flow; however, in reality, even this

portion of the aeroshell would be exposed to aerodynamic heating and would require thermal protection. Additionally, a calculation of surface curvature would be required to capture trends in local heat rates associated with shape change, particularly for a slender, lifting configuration

Because these objectives conflict, multiobjective optimization techniques may be applied to consider several objectives simultaneously while satisfying all necessary constraints. Given a set of mission requirements that define constraints (such as *L/D*, volume, and size), the aeroshell shape can be optimized in a multiobjective sense. The design variables are the locations of the control points of the NURBS surface and the AOA. The range of possible solutions is limited by size and volume constraints. Terms that represent the CG offset, static stability, and aeroshell structure and TPS masses are included as objectives to minimize the CG offset required for static trim, maximize the static stability, and minimize the mass of the aeroshell, respectively. The iSIGHT software by Engineous is used to create the environment for aeroshell shape optimization, taking advantage of its built-in version of the NSGA-II[9] multiobjective genetic algorithm. Within this integrated environment are MATLAB modules that were developed to perform shape generation, aerodynamic analysis, and objective function evaluation.

Using this integrated optimization environment, Pareto fronts can be generated for any combination of conflicting objectives. Note that if a pair of objectives does not conflict, then the dimensionality of the objective space can be reduced by eliminating one of those objectives from the multiobjective optimization. Along the Pareto front are designs for which no single objective can be improved without degrading another. With such solutions in hand, the designer can quantify the trade-offs between the various designs in terms of the objectives.

V. Results

The Mars Science Laboratory (MSL) aeroshell was chosen as a baseline with which to explore the capabilities developed in this work. Aerodynamic and geometric constraints were derived from published MSL geometry and mission requirements.[9]

An analytic, MSL-derived aeroshell is shown in Fig. 5, along with parameters computed from a Newtonian hypersonic aerodynamic analysis. It has a 70° sphere-cone forebody with a conical backshell, designed to fly at a non-zero AOA, thereby producing an *L/D* of 0.24. Note that the actual MSL backshell has a biconic geometry – the single conical frustum used here has an equivalent volume. There is a maximum-diameter constraint of 4.5 m dictated by the diameter of the launch vehicle fairing and the size of the integration and test facilities at the Jet Propulsion Laboratory. An equivalent aeroshell volume requirement of approximately 18 m^3 was determined from the present MSL design. A maximum-length constraint was determined based on the length of the MSL aeroshell, with a forebody length of approximately 0.75 m and a backshell length of approximately 2 m. Thus, an optimized aeroshell is required to fit within a 4.5-m diameter by 2.75-m circular cylinder, have a volume of 18 m^3, and achieve an *L/D* of 0.24.

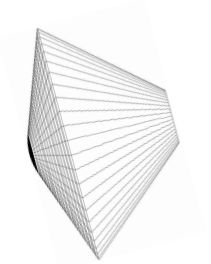

α_{trim} = -15.5°
L/D = 0.24
Volume = 18 m^3

Parameter	Value
C_DA	25.56 m^2
$(C_mAl)_\alpha$	-12.18 m^3/rad
η_V	0.7343

Figure 5. Analytic baseline aeroshell.

All of these constraints are to be met by the multiobjective optimization problem; however, equality constraints can cause difficulty in producing a diverse set of feasible, Pareto-optimal solutions. Population-based, evolutionary multiobjective algorithms – like NSGA-II – are fundamentally unconstrained optimization algorithms. Equality constraints in a multiobjective optimization problem require the optimizer to locate individual solutions that have very specific characteristics. Additionally, the solutions that meet these strict criteria must be non-dominated with respect to one another in order to form a Pareto-optimal set. If the equality constraints are difficult to meet – that is, if feasible solutions are widely dispersed over the design space – the result is likely to be an entire population of Pareto-optimal solutions that are crowded around a single design, deviating only within the allowable constraint violation tolerances. To avoid this issue, each equality constraint can be converted into two inequality constraints, with an acceptable margin added to the desired constraint value. In this work, the MSL-derived volume and *L/D* equality constraints were both relaxed by 10% of the original equality constraint value. In particular, volume was constrained between 18 m^3 and 19.8 m^3 and *L/D* was constrained between 0.24 and 0.264.

In order to highlight the trade-offs associated with this particular application, the following three objectives were emphasized for aeroshell shape optimization: drag-area, static stability, and volumetric efficiency. The analytic baseline aeroshell shown in Fig. 5 was analyzed using the same Newtonian aerodynamics routine that would be employed for optimization. First, the trim AOA required to produce an *L/D* of 0.24 was determined. At this trim

AOA, the drag-area, static stability derivative, and volumetric efficiency were computed. These values then served as a baseline against which to compare solutions produced through optimization.

A. Single Objective Optimization

Initially, optimal solutions were computed using a single objective genetic algorithm within iSIGHT in order to investigate the bounding cases for these three objectives. Figure 6 shows the results from the three single objective optimizations and includes comparisons to the analytic baseline that is shown in Fig. 5.

The maximum drag-area solution (see Fig. 6a) resulted in an aeroshell with a flat plate forebody, as expected. The aeroshell trims at an AOA that produces the required *L/D* and then the backshell fulfills the volume constraint. Since a Newtonian aerodynamic analysis is performed, the actual shape of the backshell is arbitrary as long as its size satisfies the volume constraint. This solution also gives the maximum improvement in drag-area that we can expect over the analytic baseline. The increase in drag-area of approximately 14% translates into a decrease in β by the same percentage, as shown by Eq. (1) for a given *m*. Both the static stability and the volumetric efficiency have worsened relative to the analytic baseline, with the largest adverse impact being on stability (drag has been improved to the point that this aeroshell is statically unstable).

The aeroshell that maximizes static longitudinal stability will have the largest negative value of $(C_M AL)_\alpha$ since this quantity takes on a negative value for statically stable configurations. Figure 6b shows the solution obtained from the single objective optimization to maximize static stability. Contrary to the maximum drag-area solution, the bulk of the volume has been shifted into the forebody, giving the aeroshell a more slender, swept character. As expected, the two ignored objectives have worsened relative to the analytic baseline. The resulting drag-area decrement translates directly into an approximately 30% increase in β for a given *m*.

Finally, the solution for maximizing the volumetric efficiency alone is shown in Fig. 6c. Because the volume of the aeroshell is set as a constraint, maximizing the volumetric efficiency is equivalent to minimizing the surface area of the aeroshell (see Eq. (3)). The resulting solution has a very high volumetric efficiency that is achieved through the ellipsoidal shape of the aeroshell. Furthermore, the optimizer is able to achieve a higher volumetric efficiency at the lower end of the volume constraint (18 m^3) Note that while a sphere aeroshell would have the maximum volumetric efficiency, the *L/D* constraint forces deviation from an actual sphere. A right, circular cylinder would be the aeroshell with the minimum volumetric efficiency in the current design space. Once again, the other two objectives have been significantly worsened by optimizing only a single objective.

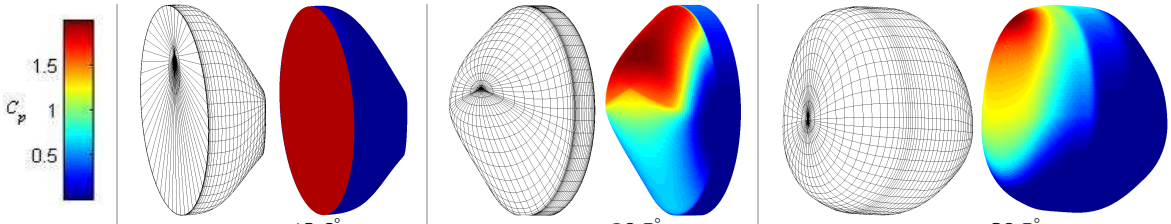

Parameter		a) maximum drag-area		b) maximum stability		c) maximum volumetric efficiency	
		α_{trim} = -13.6°		α_{trim} = -28.5°		α_{trim} = -38.5°	
		L/D = 0.240		*L/D* = 0.241		*L/D* = 0.240	
		Volume = 19.0 m^3		Volume = 18.1 m^3		Volume = 18.0 m^3	
		Value	% Difference	Value	% Difference	Value	% Difference
$C_D A$	m^2	29.20	+14.27%	17.69	-30.77%	8.321	-67.44%
$(C_m Al)_\alpha$	m^3/rad	0.4900	+104.02%	-19.49	-60.03%	-1.049	+91.39%
η_V		0.6938	-5.52%	0.6645	-9.51%	0.9806	+33.54%

Figure 6. Solutions for single objective optimizations (aeroshell meshes are shown coarse for clarity).

B. Multiobjective Optimization

As shown using single objective optimization, the chosen objectives conflict in terms of finding an optimal aeroshell shape. For such conflicting objectives, many optimal solutions exist until explicit preferences are defined for each objective. In terms of design selection, it is best to have in hand the set of Pareto-optimal solutions that quantify the trade-offs between objectives. The solutions obtained in the previous section represent extremes along these Pareto fronts. Using a multiobjective genetic algorithm in iSIGHT (NSGA-II), sets of Pareto-optimal solutions were generated for each pair of objectives. Each Pareto-optimal set of solutions is shown below in Figs. 7-10, along

with the single objective optimization results and the analytic baseline for comparison. For each pair of objectives, an arrow indicates the direction of overall improvement.

Figure 7 shows the Pareto-optimal set of solutions that simultaneously maximizes aeroshell drag-area and static stability. (Recall that static stability is increased as $(C_M Al)_\alpha$ becomes a larger negative value.) Starting with the maximum static stability solution and moving rightward along the Pareto front, static stability is given up for an improvement in drag-area. This trade-off is gradual at first, but then increases rapidly until the maximum drag-area solution is reached. In terms of aeroshell shape, the trade-off of static stability for drag-area is due to a gradual blunting of the forebody and an attendant shift of volume into the backshell. Note that the analytic baseline does not lie along the Pareto front – it is a solution that is dominated by all the other Pareto-optimal solutions. A 90° arc drawn from the analytic baseline solution toward the Pareto front illustrates that Pareto-optimal solutions within this arc yield an improvement in *both* objectives over that of the analytic baseline.

Figure 8 shows the Pareto-optimal set of solutions that simultaneously maximizes aeroshell drag-area and volumetric efficiency. Compared to the Pareto front in Fig. 7, this Pareto front extends over a much larger range of drag-area values. In general, the sacrifice in drag-area required to obtain aeroshells with maximum volumetric efficiency is much greater than the sacrifice in drag-area required to obtain aeroshells with maximum static stability. In terms of aeroshell shape, aeroshells with high volumetric efficiency tend to lack broad, flat surface areas that are characteristic of aeroshells with high drag-area. Consequently, aeroshells with higher volumetric efficiency have a lower drag-area. Once again, there is again a segment of the Pareto front within which an improvement can be made to both the drag-area and volumetric efficiency, relative to the analytic baseline aeroshell (as indicated by the 90° arc drawn).

Finally, Fig. 9 shows the Pareto-optimal set of solutions that simultaneously maximizes aeroshell volumetric efficiency and static stability. The trade-off in static stability for increasing volumetric efficiency is similar to that for increasing drag-area, with approximately the same range of static stability covered in both cases. In terms of aeroshell shape, starting from an aeroshell with high static stability, increasing volumetric efficiency will cause expansion of both the forebody and backshell. Similar to when drag-area is increased, the shift of volume to the backshell has a destabilizing effect. As shown by the 90° arc drawn, there are solutions along the Pareto front which provide improvement in both volumetric efficiency and static stability, relative to the analytic baseline aeroshell.

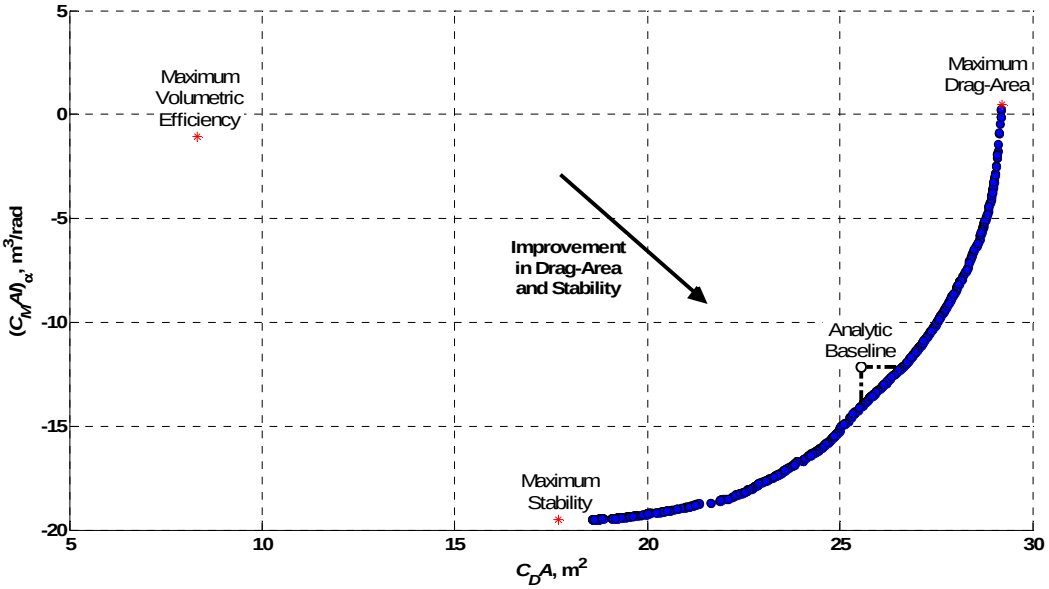

Figure 7. Pareto-optimal solutions for maximizing drag-area and maximizing stability.

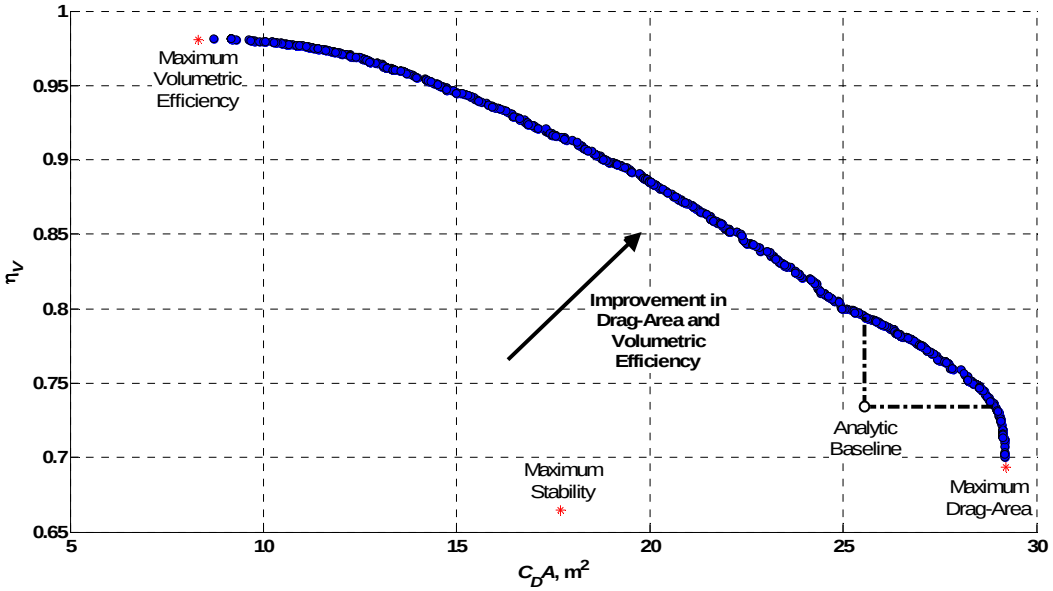

Figure 8. Pareto-optimal solutions for maximizing drag-area and maximizing volumetric efficiency.

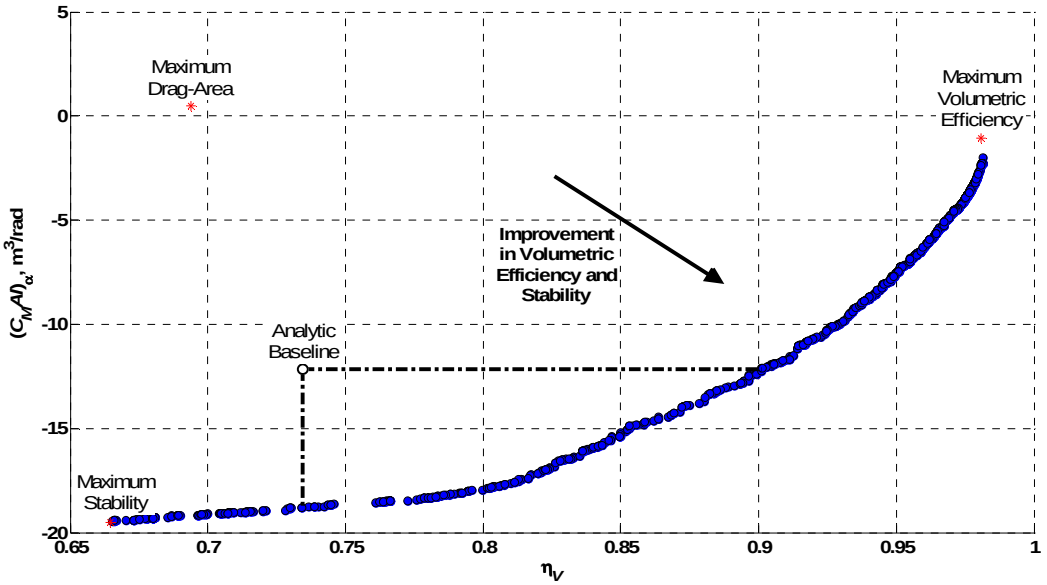

Figure 9. Pareto-optimal solutions for maximizing volumetric efficiency and maximizing stability.

As previously indicated, there is a segment along each Pareto front that contains solutions providing improvement in both objectives, relative to the analytic baseline shown in Fig. 5. In order to investigate this aspect of the objective space, a single design was selected from each Pareto front segment and the three resulting designs are shown in Fig. 10. As in Fig. 6, the objectives for each aeroshell are compared to that of the analytic baseline through a percent difference. The design in Fig. 10a shows an improvement in both drag-area and static stability, with greater improvement in static stability. Relative to the analytic baseline, the forebody has been blunted slightly and the backshell has gotten shallower – increasing both the drag-area and static stability, respectively. Note that the volumetric efficiency has been degraded. Figure 7 shows that if the static stability was made no worse than that of the analytic baseline, the drag-area could be increased by approximately 4% – a magnitude that would likely decrease once other objectives are considered. Next, Fig. 10b shows an aeroshell that provides an improvement in both drag-area and volumetric efficiency. Compared to the analytic baseline, this aeroshell has a blunter forebody that increases drag-area and a backshell with a more rounded character that serves to increase the overall volumetric

efficiency. Note that a portion of this increased volumetric efficiency is likely due to the increase in volume: this aeroshell has reached the upper limit of that constraint, set at 19.8 m^3. The static stability of this aeroshell has been degraded rather significantly compared to the analytic baseline. Finally, Fig. 10c shows an aeroshell that provides simultaneous improvement in both volumetric efficiency and static stability. The drag-area has been degraded significantly as volume has been shifted into the forebody, thus providing greater static stability, better volumetric efficiency, but less surface area that is blunt to the freestream. The backshell is shallow and swept – a hybrid of the two backshells shown in Figs. 10a and 10b – since stability and volumetric efficiency are the primary drivers of backshell shape. Note, once again, that the volume of the aeroshell has approached the upper boundary of the volume constraint, providing some of the improvement in volumetric efficiency over the analytic baseline. Overall, however, the internal volume is being used more efficiently in terms of Eq. 3.

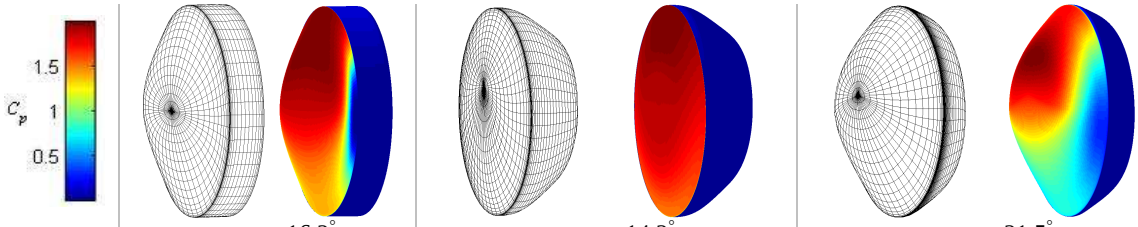

α_{trim} = -16.2°
L/D = 0.241
Volume = 18.6 m^3

Parameter		Value	% Difference
C_DA	m^2	25.81	+0.98%
$(C_mAl)_\alpha$	m^3/rad	-13.59	-11.58%
η_V		0.6780	-7.67%

a) drag-area and stability

α_{trim} = -14.2°
L/D = 0.241
Volume = 19.8 m^3

Value	% Difference
28.04	+9.73%
-7.99	+34.40%
0.7590	+3.36%

b) drag-area and volumetric efficiency

α_{trim} = -21.5°
L/D = 0.252
Volume = 19.6 m^3

Value	% Difference
18.04	-29.42%
-15.43	-26.73%
0.8466	+15.28%

c) volumetric efficiency and stability

Figure 10. Pareto-optimal solutions representing simultaneous improvement in pairs of objectives.

From the above discussion, it is clear that designs exist which offer improvement over the analytic baseline in terms of each pair of objectives. The natural progression is then to determine whether designs exist which offer improvement in all three objectives. This question was answered by performing multiobjective optimization using all three objectives with three additional inequality constraints: each objective was required to provide a performance at least as good as that of the analytic baseline design shown in Fig. 5. Figure 11 displays the results of this optimization, along with an example design from this set of solutions. Each solution represents an improvement over the analytic baseline in terms of all three objectives and is Pareto-optimal with respect to every other solution. Based on Fig. 11, the trade-offs among the three objectives are consistent with the trade-offs identified by optimizing each pair of objectives independently. The strongest trade-off here is between drag-area and static stability: for a given volumetric efficiency, the decrease in static stability as drag-area increases is greater than the decrease in static stability as volumetric efficiency increases at a given drag-area. Further investigation into these results showed that most of the improvements in volumetric efficiency corresponded to an increase in volume – essentially, the optimizer exploited the flexibility built into the volume constraint. The example solution shown in Fig. 11 has a volume close to that of the analytic baseline and shows a small improvement in all three objectives. The aeroshell forebody is similar to that of a spherical segment, but has a slightly elliptical contour near the nose. The backshell is more rounded and shallower than that of the analytic aeroshell, providing greater static stability and volumetric efficiency. The Pareto set shows that, approximately, a 4% increase in drag-area is expected to be the maximum achievable improvement over the analytic baseline without degrading the other objectives. This result is consistent with the maximum achievable improvement in drag-area that was predicted from Fig. 7. Correspondingly, the maximum improvement in static stability is expected to be approximately 12.5% and the maximum improvement in volumetric efficiency is expected to be approximately 6%. As shown in Fig. 11, many (Pareto-optimal) solutions exist that provide improvements intermediate to these expected maxima – the selection of a particular compromise solution will depend on the preferences of the designer and the specific mission requirements.

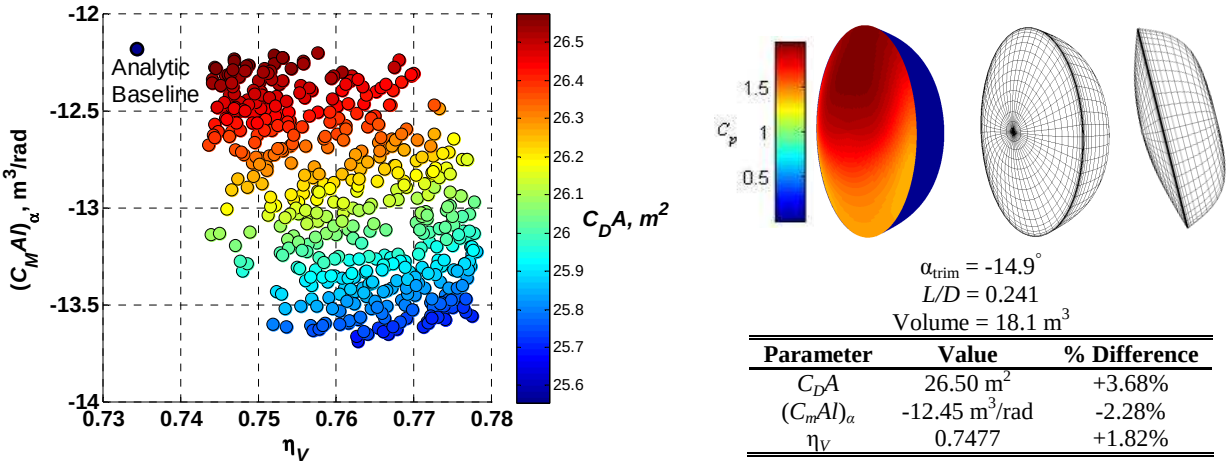

Parameter	Value	% Difference
$C_D A$	26.50 m^2	+3.68%
$(C_m Al)_\alpha$	-12.45 m^3/rad	-2.28%
η_V	0.7477	+1.82%

Figure 11. Pareto-optimal solutions representing simultaneous improvement in all three objectives.

VI. Conclusions and Future Work

A capability to perform multiobjective aeroshell shape optimization based on Newtonian hypersonic aerodynamics has been developed. Several different methods for shape parameterization have been investigated, including analytic and synthetic shapes. Synthetic, or spline, surface formulations are used to represent the aeroshell shapes because such forms allow a large diversity of smooth-bodied shapes while maintaining a relatively low number of control points (or design variables) for optimization. In particular, NURBS surfaces provide an ideal geometric representation of complete aeroshells.

An optimization framework has been created (using iSIGHT) that enables use of multiobjective evolutionary algorithms to generate Pareto-optimal sets of solutions. Objectives and constraints are determined based on aerodynamics and the geometry of the aeroshell. They include, but are not limited to, *L/D*, drag-area, static stability, volumetric efficiency, CG offset, volume, and overall aeroshell size. After deriving design constraints based on the MSL mission, single- and multiobjective optimization was performed using drag-area, static stability, and volumetric efficiency objectives. Results revealed solutions that offer improvement in these objectives relative to the analytic 70° sphere-cone, which has been employed by all U.S. robotic Mars missions. These sets of Pareto-optimal solutions also served to highlight the fundamental trade-offs between drag-area, static stability, and volumetric efficiency.

The natural progression for this work is to add objectives that can account for the impact of TPS mass on aeroshell shape design. Specifically, this step will require relations between the local surface shape and convective and radiative heating. Stagnation-point heating is typically estimated using an effective nose radius; however, it would be more complete to account for heating away from the stagnation-point as well. The most obvious choice is to relate convective heating to local surface curvature along streamlines emanating away from the stagnation point. Radiative heating relations typically require an estimate of shock stand-off distance. It is not immediately clear how to estimate the shock stand-off distance along the entire aeroshell body, but such a relation will likely depend on local surface curvature as well. In terms of exploring the design space for other EDL missions, *L/D* will be parameterized and varied from a low value, say 0.3, to a high value, say up to 1.0. For each *L/D*, a different multiobjective optimization will be performed, giving not only sets of trade-off solutions for each *L/D*, but also aeroshell trend information across the range of *L/D*. Such information will be valuable to designers of future planetary EDL missions for which lifting aeroshells are an enabling component of the overall EDL architecture.

Acknowledgments

This research was supported through a contract with the NASA ARMD Fundamental Aeronautics Program Hypersonics Project for High Mass Mars Entry System research. The input and guidance provided by Mark Schoenenberger of NASA Langley Research Center is greatly appreciated.

References

[1] Braun, R. D. and Manning, R. M., "Mars Exploration Mars Exploration Entry, Descent and Landing Challenges," Paper 1076, 2006 IEEE Aerospace Conference, Big Sky, Montana, March 2006.

[2] Mitcheltree, R. A., DiFulvio, M., Horvath, T.J., and Braun, R. D., "Aerothermal Heating Predictions for Mars Microprobe," AIAA Paper No. 98-0170, Jan. 1998.
[3] Syvertson, C. A., "Research Problems in Atmosphere Entry and Landing for Manned Planetary Missions," NASA TN D-4977, Jan. 1969.
[4] Jones, J.J., "The Rationale for an Aeroassist Flight Experiment," AIAA Paper 87-1508, June 1987.
[5] Anderson, J.D., Hypersonic and High Temperature Gas Dynamics, AIAA Education Seris, AIAA, Reston, VA, 2000, pp. 46-50.
[6] Bartels, R. H., Beatty, J. C., and Barsky, B. A., An Introduction to Splines for Use in Computer Graphics and Geometric Modeling, Morgan Kaufmann Publishers, Inc., San Mateo, CA, 1987, pp. 25-45, 46-63, 211-213.
[7] Ashley, H. and Landahl, M., Aerodynamic of Wings and Bodies, Addison-Wesley, Reading ,MA, 1965.
[8] Edquist, K. T., Prabhu, R. K., Hoffman, D. A., and Rea, J. R., "Configuration, Aerodynamics, and Stability Analysis for a Neptune Aerocapture Orbiter," AIAA Paper 2004-4953, August 2004.
[9] Deb, K., Agrawal, S., Pratap, A., and Meyarivan, T., "A Fast Elitist Non-dominated Sorting Genetic Algorithm for Multi-objective Optimization: NSGA-II," Proceedings of the Parallel Problem Solving from Nature VI, 2000, pp. 849-858.
[10] Edquist, K. T., Dyakonov A. A., Wright, and M. J., Tang, C. Y., "Aerothermodynamic Environments Definition for the Mars Science Laboratory Entry Capsule," AIAA Paper No. 2007-1206, Jan., 2007.